Catalysis Today 147 (2009) 255–259

Contents lists available at ScienceDirect

Catalysis Today

journal homepage: www.elsevier.com/locate/cattod

Investigation of the thiotolerance of metallic ruthenium nanoparticles: A XAS study

Juliette Blanchard [a,*], Kyoko K. Bando [b], Michèle Breysse [a], Christophe Geantet [c], Michel Lacroix [c], Yuji Yoshimura [b]

[a] Laboratoire de Réactivité de Surface, LRS, UMR-CNRS 7609, Université Pierre et Marie Curie-Paris6, 4 place Jussieu, 75252 Paris, France
[b] National Institute of Advanced Industrial Science and Technology, Ibaraki 305-8565, Japan
[c] IRCELYON, UMR-CNRS 5256, Université Claude Bernard Lyon 1, 2 av A. Einstein, F-69626 Villeurbanne Cedex, France

ARTICLE INFO

Article history:
Available online 18 December 2008

Keywords:
EXAFS
XANES
Ruthenium
Sulfur tolerance
Sulfur resistance
Thioresistance

ABSTRACT

In situ XAS at the Ru K edge was used to investigate the thiotolerance of metallic ruthenium supported on partially dealuminated acidic Y zeolite (Ru°/HYd, obtained by reduction at 673 K of $Ru(NH_3)_6^{3+}$/HYd). After 3 h at 523 K under 350 ppm H_2S in H_2 the formation of 1.9 Ru–S bond per Ru atoms is observed without modification of the core of the metallic particles (the number of Ru neighbors is unchanged). These results are compared to those obtained after reductive sulfidation of the same sample in order to understand the origin of the high hydrogenation activity of metallic ruthenium in the presence of H_2S.

1. Introduction

Although most of the developments on hydrotreating process and catalysts were focussed on sulfur removal (hydrodesulfurization, HDS) and nitrogen removal (hydrodenitrogenation HDN), aromatics hydrogenation has been of increasing importance for diesel specification. Especially, aromatic content and cetane number of diesel fuel, closely related to the mono and poly-aromatics concentration, are submitted to legislation.

Noble metal catalysts are generally utilized for the hydrogenation of aromatics. However, these catalysts are known to be very sensitive to sulfur and nitrogen compounds present in diesel streams and, consequently, many studies have been devoted to the increase of their thiotolerance. The utilization of an acidic support or the addition of a second metal like Pd have improved the sulfur tolerance [1–8].

Factors influencing the thioresistance of nickel catalysts in aromatics hydrogenation were also, recently examined by Pawelec et al. [9]. These authors pointed out the importance of a good balance between metal and acid sites.

Sulfide catalysts might also be considered for the hydrogenation of aromatics in the presence of sulfur. Harvey and Matheson [10] were the first to show that ruthenium sulfide dispersed in Y zeolites was very active for the hydrogenation reactions. Later, some of the present authors made an extensive study of the properties of ruthenium sulfide clusters encaged in various Y zeolites [11] and examined the influence of the acidic properties of the supports. These catalysts kept outstanding hydrogenation properties in the presence of large amounts of H_2S (1.85% H_2S in H_2). Characterization by physicochemical techniques, especially EXAFS, suggested that the active phase was composed of nanometric clusters of a ruthenium sulfide like phase with very small domains of ruthenium metal [12].

These hypotheses were confirmed recently [13] using *in situ* XAS during sulfidation of $[Ru(NH_3)_6]^{3+}$ supported on a partially dealuminated Y zeolite (HYd). It was shown that reductive sulfidation of the precursor in presence of a mixture of 15% H_2S/H_2 started at room temperature and was complete at 373 K. At that temperature, the sample was fully sulfided (5.9 S neighbours per Ru). Above 423 K a partial sulfur reduction (4.3 S neighbours per Ru) and the formation of metallic ruthenium (3.3 Ru neighbours per Ru) were observed. Upon addition of toluene, the intensity of Ru–Ru peak in the FT EXAFS spectra was modified, whereas the Ru–S peak remained unchanged. This suggested that the chemisorption of toluene occurred on the metallic domains and showed the prominent role of these sites for aromatics hydrogenation. The high activity of these metallic sites (compared to metallic ruthenium) was assigned to an electronic effect of the RuS chore on the supported Ru° domains.

* Corresponding author. Tel.: +33 144273630; fax: +33 144276033.
E-mail address: juliette.blanchard@upmc.fr (J. Blanchard).

0920-5861/$ – see front matter © 2008 Elsevier B.V. All rights reserved.
doi:10.1016/j.cattod.2008.10.033

Another remarkable property of ruthenium supported on zeolite is its thiotolerance. Indeed, whereas the addition of H_2S to the feed drastically decreases the hydrogenation activity of metallic platinum and palladium [14], ruthenium is able to preserve most of its hydrogenation activity in presence of sulfur. It has indeed been reported that Ru° supported on Y zeolite keeps about 3/4 of its hydrogenation activity (tetraline hydrogenation) after exposure to 330 ppm H_2S/H_2 [15]. Under these conditions, the hydrogenation activity of Ru°/HYd remains nevertheless about 8 times lower than that of RuS_x/HYd.

In order to understand the relationship between the active phase obtained after reductive sulfidation and that formed after reduction and poisoning, we have used *in situ* EXAFS to examine the properties of a Ru°/HYd catalyst before and after exposure to H_2S.

2. Experimental

2.1. Catalyst preparation

The $[Ru(NH_3)_6]^{3+}$/HYd sample was prepared as described in [16]. The acidic dealuminated Y zeolite (HYd) used as support has the following characteristics: Si/Al = 13.6 ($Si/Al_{framework}$ = 19 determined using ^{29}Si NMR), S_{BET} = 802 $m^2\,g^{-1}$. The Ru loading as determined by chemical analysis is 1.5 wt%.

2.2. Characterization

2.2.1. HRTEM

Samples were reduced beforehand under pure H_2 at 673 K during 2 h (heating rate 1 K min^{-1}). High resolution transmission electron microscopy measurements were performed on a Jeol JEM 2010 microscope. The mean particle size was calculated from ca. 100 particles using the d_{VA} formula (volume area mean diameter) [17].

$$d_{VA} = \frac{\sum n_i d_i^3}{\sum n_i d_i^2}$$

2.2.2. CO chemisorption

CO chemisorption was used to determine the Ru° particle size and the effect of exposure to H_2S on the number of metallic sites. The total amount of CO chemisorbed on Ru°/HYd was determined using the CO pulse adsorption method. ca. 100 mg of the sample was reduced *in situ* in pure H_2 (30 $cm^3\,min^{-1}$) at 673 K for 2 h (heating rate 1 K min^{-1}) and then purged by He at the same temperature for 10 min. Pulses (0.5 cm^3) of 10.1% CO (in He) were injected into a stream of He carrier gas (30 $cm^3\,min^{-1}$) and contacted with the catalyst at 323 K. The amount of chemisorbed CO was analyzed by a thermal conductivity detector and the dispersion was calculated as follows:

$$\mathrm{Dr} = \frac{\text{total amount of adsorbed CO (mol g}^{-1})}{\text{total amount of supported metal (mol g}^{-1})} \times 100\,(\%)$$

The average metal particle size was estimated using the equation $d_{VA} = 6v_m/(a_m D)$ where d_{VA} is volume area mean diameter, v_m is the volume occupied by an atom in bulk metal (13.65 $Å^{-3}$ for Ru) and a_m is the surface occupied by a surface atom (6.35 $Å^{-2}$ for Ru).

To study the effect of H_2S, the same measurement was performed, except that after *in situ* reduction in H_2, the sample was exposed to a 500 ppm H_2S/H_2 stream at 523 K during 1 h before the addition of the CO pulses.

2.2.3. XAS

A wafer of dried [Ru(NH_3)6]3$^+$/HYd (200 mg, 10 mm in diameter) was set in an *in situ* cell designed for high temperature (up to 873 K) measurements under a reactant gas [18] and reduced under H_2 (flow rate: 100 ml/min) at 673 K during 1 h (heating rate 5 K min^{-1}). After reduction the temperature was decreased to 523 K, the gas flow switched to 350 ppm H_2S/H_2 for 3 h and to 2% H_2S/H_2 for 2 h. The Ru K-edge (22.1 keV) EXAFS and XANES spectra were measured at Photon Factory (Institute for Material Structure Science, High Energy Accelerator Organization, KEK-IMSS-PF, Japan) on beamline 10 B using a channel-cut monochromator. The transmission spectra were collected using ionization chambers filled with Ar and Kr for I_0 and I, respectively. Spectra were measured at 523 K after reduction (Ru°/HYd), after 3 h under 330 ppm H_2S/H_2 (Ru°/HYd-330 ppm) and after 2 h under 2% H_2S/H_2 (Ru°/HYd-2%)

The extraction of the EXAFS oscillation was performed as described in [13] using Athena software [19,20]. The curve fitting analysis was performed with Artemis software [19,20], over a k range of 3–14 $Å^{-1}$ and a R range of 1.2–3 Å. The maximum number of independent points can be estimated from the expression $IP = [(2\,\Delta k\,\Delta R/\pi) + 1]$, where Δk is the extent of the data in k-space and ΔR the R range to be modelled. The number of variables used for the analysis (8) remained well below the number of independent points (IP = 12).

The fit of the experimental data were performed as described in [13], using theoretical paths generated by the Atoms 2.5 [21] and FEFF 8.0 [22]. The passive electron reduction factor S_0^2 was determined experimentally on metallic ruthenium ($S_0^2 = 0.79$).

2.2.4. Tetralin hydrogenation

Detailed experimental conditions are given in [15]. Briefly, prior to catalytic test the samples were either reduced under pure H_2 or sulfided (15%H_2S/H_2) at 673 K under atmospheric pressure. Reaction was performed in an open high-pressure microreactor working in the gas phase (P_{H_2} = 4.5 MPa and $P_{tetralin}$ = 2.7 KPa, P_{H_2S} = 1.48 kPa or 0) at 523 K. After a first period of rapid deactivation, the catalyst deactivate very slowly. The specific rates were measured after a steady state was reached that is after18 h time on stream (a typical deactivation curve can be seen in [12]. The specific activity of Ru°/HYd in absence of sulfur was 1.8 10^{-7} mol s^{-1} g^{-1}. It decreased to 1.3 × 10^{-7} mol s^{-1} in presence of H_2S. The activity of RuS_x/HYd in the same conditions was 12 × 10^{-7} mol s^{-1} g^{-1}.

3. Results and discussion

3.1. Characterization of the Ru° particles

Fig. 1 shows the HRTEM micrograph of Ru°/HYd. Small Ru° clusters can be detected with a diameter ranging between 15 and 25 Å. The volume area mean diameter of the particles is 20 Å. The dispersion measured by CO chemisorption is 86% which corresponds to a mean particle size of 15 Å. This value is significantly smaller than the average particle size measured by HRTEM, which could indicate that very small Ru° particles (≤1 nm) are also present that could not be detected using TEM.

The XANES spectra of Ru°/HYd at the Ru K edge is compared with those of $[Ru(NH_3)_6]^{3+}$/HYd and bulk Ru° (Fig. 2). The shift in the position of the edge between $[Ru(NH_3)_6]^{3+}$/HYd and Ru°/HYd (from 22,130 to 22,118 eV) is a clear indication of the reduction of ruthenium. The XANES spectrum of Ru°/HYd is similar to that of Ru° except that the XANES modulations have smaller amplitude and are slightly shifted. According to Bazin et al. [23], these differences arise from the nanometric size of the metallic particles in Ru°/HYd.

The EXAFS spectrum ($FT(k^3\chi(k))$) of Ru°/HYd is shown in Fig. 3 together with those of $[Ru(NH_3)_6]^{3+}$/HYd and Ru°. The EXAFS signal

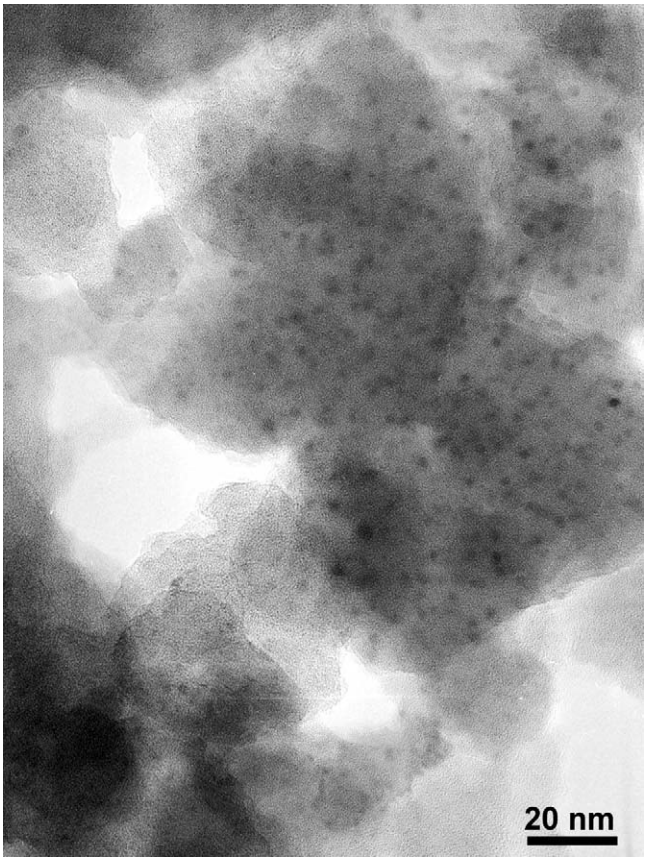

Fig. 1. TEM micrograph of Ru°/HYd.

of $[Ru(NH_3)_6]^{3+}$/HYd is characteristic of N (or O) neighbours at 2.13 Å (observed at 1.69 Å in Fig. 3 in the absence of phase correction) and an average coordination of 5 is determined by the fit. The position of the main peak is shifted upon reduction and is characteristic of the formation of metallic ruthenium with Ru neighbours at 2.67 Å (observed at 2.36 Å in Fig. 3 in the absence of

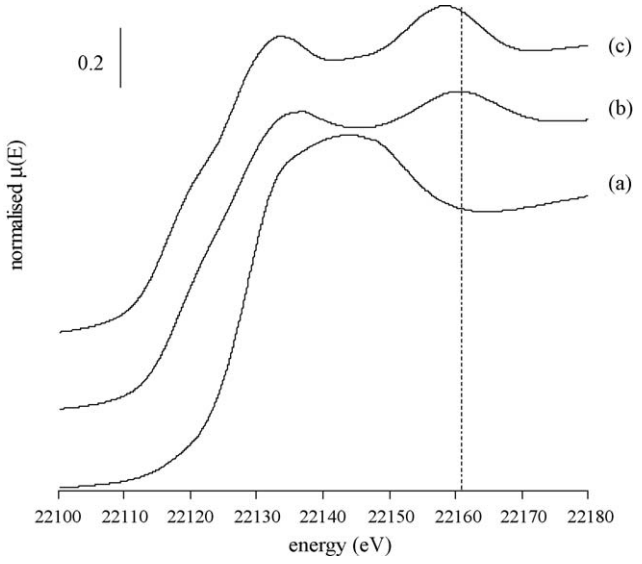

Fig. 2. XANES spectra of the EXAFS spectra of (a) $[Ru(NH_3)_6]^{3+}$/HYd; (b) same sample after reduction under H_2 at 673 K (straight line); and (c) bulk Ru°. Spectrum (a) was recorded at room temperature under He; spectra (b) and (c) were recorded at 523 K under H_2.

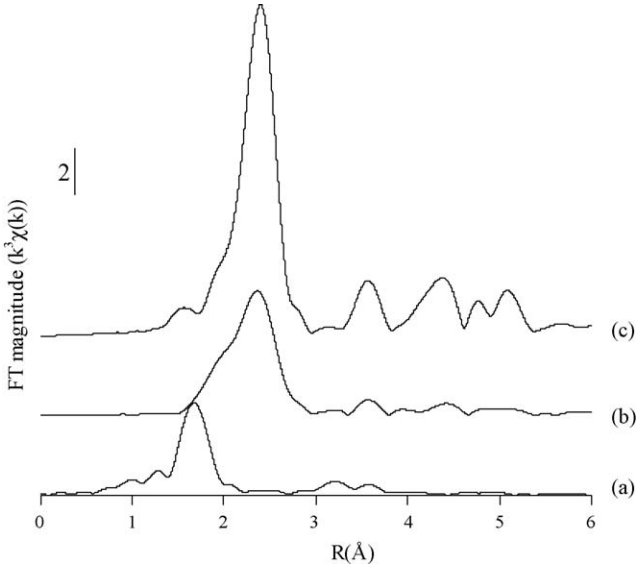

Fig. 3. FT($k^3\chi(k)$) of the EXAFS spectra of (a) $[Ru(NH_3)_6]^{3+}$/HYd; (b) same sample after reduction under H_2 at 673 K (straight line); and (c) bulk Ru°. Spectrum (a) was recorded at room temperature under He; spectra (b) and (c) were recorded at 523 K under H_2.

phase correction). The amplitude of this peak is nevertheless much lower for Ru°/HYd than for bulk Ru°, which is a confirmation of nanoparticles formation. Moreover the shoulder at ca. 2 Å indicates the presence of O neighbours. As previously reported by Koningsberger and coworkers for metallic Pt° nanoparticles supported on nonreducible metal oxide supports [24,25] it was necessary to include two O shells, one at 2.13 and the other at 2.46 Å. However a fit with three shells (2 O and 1 Ru) would involve 12 variables, a value too close to the number of independent points. For this reason, two spectra recorded at two different temperatures (523 and 673 K) were simultaneously fitted, leading to a number of independent points of 24 and a number of variables of 12 (for each shell the number of neighbours, their distance, the shift in E_0 were kept the same for the two spectra and the variation of the Debye Waller factor with temperature was estimated as reported in [13]. The value of the fit reported in Table 1 indicate the presence of about 2 O neighbours per central Ru with a majority of O neighbours at long distance (0.7 at 2.13 Å and 1.2 at 2.46 Å). Note that there is a large uncertainty on these values that could therefore be overestimated.

The presence of O neighbours at long distance was reported by Koningsberger and coworkers after mild reduction (T_{red} = 573 K) whereas O neighbours at short distance were observed after high temperature reduction (T = 873 K); at intermediate reduction temperature both contributions were present [24]. The short metal oxygen distance is, according to these authors characteristic of support oxygen atoms in contact with zero-valent metal clusters (this distance is slightly higher than the metal oxygen distance in metallic oxide d_{Ru-O} = 1.99 Å). The long metal oxygen distance is, according to these authors, due to the formation of an interfacial layer of H_2 between the zeolite and the metallic particle.

The average coordination of the Ru shell is 8.3. According to the work of de Graaf et al. an average coordination of 7.3 corresponds to platinum clusters made of 43 atoms whereas an average coordination of 8.5 corresponds to clusters made of 79 atoms (Pt particle size 16 Å) [26]. Although the crystalline structure of metallic Ru is different from that of metallic Pt (hexagonal close packed instead of cubic close packed) one can assume that the nanoparticles have the same cuboctahedric shape. Considering the

Table 1
Structural parameters from EXAFS for reference compounds (Ru(0) and RuS_2) and for $[Ru(NH_3)_6]^{3+}$/HYd zeolite after reduction and after exposure to sulfur (350 ppm and 2% H_2S in H_2). Spectra were recorded at 523 K.

	E_0 (eV)	Scatterer	N	R (pm)	σ^2 ($\times 10^{-4}$ Å^2)	ΔE_0 (eV)	R-factor (%)
Ru(0)	22,117	Ru	12	267 (1)	65	5.2 (0.2)	0.3
$[Ru(NH_3)_6]^{3+}$/HYd	22,130	N	5 (0.7)	213 (1)	33 (10)	0 (2)	1.5
RuS_x/HYd	22,125	Ru	3.5[a]	265.5 (5)	107 (5)	−8	0.7
		S	4.2 (0.4)	232.2 (0.3)	64 (2)	8	
Ru°/HYd	22,118	Ru	8.3 (0.6)	263 (1)	106 (4)	−3 (1)	0.1
		O2	1.2 (0.7)	246 (1)	13 (28)	−9 (10)	
		O1	0.7 (0.4)	213 (2)	11 (25)	−9 (10)	
Ru°/HYd	22,123	Ru	8.0 (0.7)	265 (1)	96 (5)	−7 (1)	0.2
350 ppm H_2S/H_2		S	1.9 (0.3)	232 (1)	57 (1)	−6 (2)	
Ru°/HYd	22,124	Ru	8.1 (0.8)	265 (1)	96 (6)	−7 (1)	0.4
2% H_2S/H_2		S	2.2 (0.4)	232 (1)	61 (1)	−6 (2)	

[a] The condition $N(S) + 0.5 \times N(Ru) \leq 6$ was applied.

Pt–Pt (2.77 Å) and Ru–Ru (2.65 Å) bond lengths, the size of a 79 atoms Ru cluster should be approximately 15 Å, that is the value determined by CO chemisorption. The fact that the average size of the Ru° nanoparticles is close to the size of the zeolite supercage (13 Å) and the high number of O neighbours (at short and long distance) are clear indications that most of the ruthenium nanoparticles are located in the zeolite cavities.

3.2. Characterization of Ru° nanoparticles after exposure to H_2S (350 ppm and 2% H_2S in H_2)

The metal dispersion determined after exposure to 500 ppm H_2S decreases from 86% to 17.5%. Although the decrease in the number of metallic sites upon exposure to H_2S is quite high (about 80% of metallic sites are lost), Ru°/HYd still shows a remarkable sulfur tolerance as compared to other noble metal, with a resistance to poisoning similar to that of bimetallic Pt–Pd nanoparticles supported of ultra stable Y zeolite [27].

Fig. 4 shows the XANES spectra of Ru°/HYd just after reduction, after exposure to 350 ppm H_2S in H_2 (3 h), and after subsequent exposure to 2% H_2S in H_2 (2 h). The XANES spectrum of RuS_x/HYd obtained by reductive sulfidation of $[Ru(NH_3)_6]^{3+}$/HYd at 673 K under 15%H_2S/H_2 [13] is also shown for comparison. The modification of the XANES spectrum upon exposure to H_2S is clearly visible and the spectrum of the sample exposed to 350 ppm H_2S/H_2 and 2% H_2S/H_2 are intermediary between those of Ru°/HYd and RuS_x/HYd. The edge is shifted from 2118 eV just after reduction to 2122 eV (exposure to 350 ppm H_2S/H_2) and to 2123 eV (exposure to 2% H_2S/H_2), that is close to the value of RuS_x/HYd (2125 eV). Moreover the positions of the XANES modulations are intermediary between those of Ru°/HYd and RuS_x/HYd.

The Fourier transform of the EXAFS spectra before and after exposure to H_2S are shown in Fig. 5. Exposure to 350 ppm H_2S/H_2 during 3 h does not modify the intensity of the main peak corresponding to the Ru neighbours. A shoulder, at a position similar to that of the S neighbours in RuS_x/HYd is however clearly visible. Surprisingly, subsequent exposure to 2% H_2S/H_2 does not change significantly the EXAFS spectra. The structural parameters extracted from the simulation of these spectra are reported in Table 1. These simulations confirm that the number of metallic neighbours remains unchanged upon exposure to H_2S, even for the higher H_2S partial pressure. It also shows the presence of 1.9 (after exposure to 350 ppm H_2S/H_2) and 2.2 (after exposure to 2% H_2S/H_2) S neighbours per Ru. The absence of modification of the Ru shell is a clear indication that no bulk sulfidation of the metallic nanoparticles took place even at high (2%) H_2S partial pressure. This is a major difference with other noble metal like platinum and palladium for which bulk sulfidation was evidenced by EXAFS: for example for

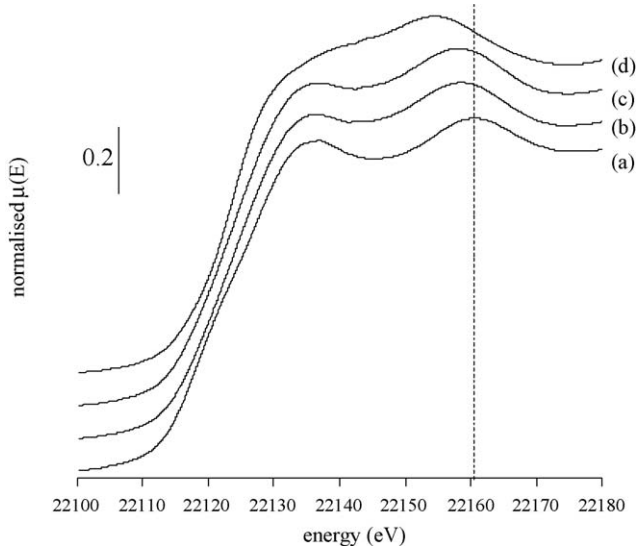

Fig. 4. XANES spectra of Ru°/HYd after reduction under H_2 at 673 K (a), after exposure to 350 ppm H_2S/H_2 (b) and to 2% H_2S/H_2 (c), and of RuS_x/HYd (reductive sulfidation at 673 K of $[Ru(NH_3)_6]^{3+}$, (d)). The three spectra were recorded at 523 K.

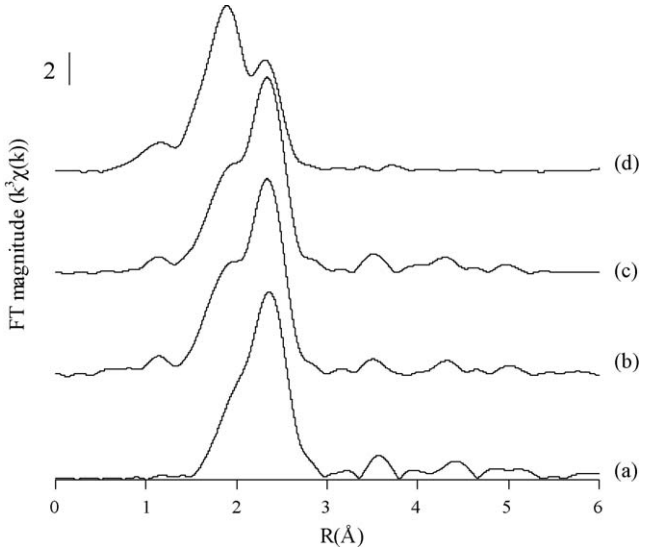

Fig. 5. FT($k^3\chi(k)$) of the EXAFS spectra of Ru°/HYd after reduction under H_2 at 673 K (a), after exposure to 350 ppm H_2S/H_2 (b) and to 2% H_2S/H_2 (c), and of RuS_x/HYd (reductive sulfidation at 673 K of $[Ru(NH_3)_6]^{3+}$, (d)). The three spectra were recorded at 523 K.

very small Pt or Pd nanoparticles (14–15 Å) supported on USY zeolite the average coordination number decreases from 7 to about 3.5 and for slightly large particles (26 Å) it decreases from 9 to 7 (Pt) or to 5 (Pd) [28]. Even for bimetallic Pt–Pd particles a bulk sulfidation of the Pd was reported [27].

Surface sulfidation is on the other side pronounced with 1.9–2.2 S neighbours per Ru. Considering the dispersion measured by CO chemisorption before poisoning (86%), it means that the average number of S neighbours per surface Ru is 2.2 after exposure to 350 ppm H_2S and 2.6 after exposure to 2% H_2S. This is consistent with the sharp decrease in CO chemisorption after exposure to H_2S (from 86% to 17.5%). After exposure to H_2S, O shells are no longer required to obtain a high quality fit. This could indicate that the O neighbours have been replaced by S neighbours. This hypothesis is also consistent with the fact that the number of O neighbours (before exposure to H_2S) and S neighbours (after exposure to H_2S) are very close (although the numbers of O neighbours must be taken with caution as the uncertainties on these values are every high).

For comparison, the EXAFS spectrum of a RuS_x/HYd sample obtained by reductive sulfidation (sulfidation at 673 K under 15% H_2S/H_2 of the same starting material, i.e. $[Ru(NH_3)_6]^{3+}$/HYd) is shown in Fig. 5. The position of the Ru–S and Ru–Ru peaks are identical to those of the spectra of Ru°/HYd after exposure to H_2S. This is confirmed by the fit of the spectra which shows identical bond length for the Ru–S and Ru–Ru bond whatever the sample. On the other side the intensities of the peak are clearly different with about 4.2 S neighbours and 3.5 Ru neighbours.

The question that remains is why the hydrogenation activity is almost completely preserved after exposure to H_2S in spite of the strong decrease in surface metallic sites (evidenced by both CO chemisorption and EXAFS). The likeliest explanation is that the electronic properties of the remaining metallic sites are modified by the surface sulfidation of the neighbouring sites, resulting in an enhancement of their activity. The active sites in Ru°/HYd after exposure to H_2S would as a consequence be closely related to those in RuS_x/HYd formed by reductive sulfidation (15% H_2S/H_2).

4. Conclusion

A Ru°/HYd sample was prepared by reduction at 673 K of $[Ru(NH_3)_6]^{3+}$/HYd. This sample was characterized just after reduction and after exposure to H_2S (350 ppm H_2S/H_2 and 2% H_2S/H_2). The characterizations (XAS, TEM and CO chemisorption) of the reduced sample reveal the formation of Ru° nanoparticles (about 15 Å) that are interacting with the zeolite framework and are therefore mostly located in the zeolite cavities. The decrease (by a factor of 5) in the number of metallic sites after exposure to H_2S is a clear indication of surface sulfidation. This is confirmed by XAS, with the presence of about 2 S neighbours per Ru (1.9 after exposure to 350 ppm H_2S and 2.2 after exposure to 2% H_2S). Moreover the fact that the number of Ru neighbours remains unchanged after exposure to H_2S indicates that Ru°, unlike other noble metals metallic nanoparticles such as Pt° and Pd°, do not undergo bulk sulfidation. These results can help to understand why Ru°/HYd keeps most of its hydrogenation activity in presence of H_2S: we propose that, after exposure to H_2S, the activity of the remaining metallic sites (ca. 20%) is increased due to a modification of their electronic properties by the neighbouring sulfided sites. FTIR of adsorbed CO [11] could be used to investigate further the nature of the surface sites of these partly sulfided clusters and especially the hypothesis of a modification of the electronic properties of metallic ruthenium in presence of H_2S.

Acknowledgments

This work was carried out in the framework of the Japanese–French GDRI ECSAW and the XAS experiments were performed under the approval of the Photon Factory Advisory Committee (proposal no. 2003G070). The authors thank the CNRS and the AIST for supporting this research.

References

[1] P. Gallezot, J. Datka, J. Massardier, M. Primet, B. Imelik, Proc. 6th ICC. A (1976) 696.
[2] A. Stanislaus, B.H. Cooper, Catal. Rev. Sci. Eng. 36 (1994) 75–123.
[3] H. Yasuda, T. Sato, Y. Yoshimura, Catal. Today 50 (1999) 63–71.
[4] R.M. Navarro, B. Pawelec, J.M. Trejo, R. Mariscal, J.L.G. Fierro, J. Catal. 189 (2000) 184–194.
[5] K. Thomas, C. Binet, T. Chevreau, D. Cornet, J.P. Gilson, J. Catal. 212 (2002) 63–75.
[6] D. Bazin, D. Guillaume, C. Pichon, D. Uzio, S. Lopez, Oil Gas Sci. Technol. 60 (2005) 801–813.
[7] D. Eliche-Quesada, J.M. Mérida-Robles, E. Rodríguez-Castellón, A. Jiménez-López, Appl. Catal. B: Environ. 65 (2006) 118–126.
[8] A. Niquille-Roethlisberger, R. Prins, Catal. Today 123 (2007) 198–207.
[9] B. Pawelec, P. Castano, J.M. Arandes, J. Bilbao, S. Thomas, M.A. Pena, J.L.G. Fierro, Appl. Catal. A 317 (2007) 20–33.
[10] T.G. Harvey, T.W. Matheson, J. Catal. 101 (1986) 253–261.
[11] M. Breysse, M. Cattenot, V. Kougionas, J.C. Lavalley, F. Mauge, J.L. Portefaix, J.L. Zotin, J. Catal. 168 (1997) 143–153.
[12] B. Moraweck, G. Bergeret, M. Cattenot, V. Kougionas, C. Geantet, J.-L. Portefaix, J.L. Zotin, M. Breysse, J. Catal. 165 (1997) 45–56.
[13] J. Blanchard, K.K. Bando, T. Matsui, M. Harada, M. Breysse, Y. Yoshimura, Appl. Catal. A: Gen. 322 (2007) 98–105.
[14] A. Renouprez, J.L. Rousset, A.M. Cadrot, Y. Soldo, L. Stievano, J. Alloys Compds. 328 (2001) 50–56.
[15] P. Tian, J. Blanchard, K. Fajerwerg, M. Breysse, M. Vrinat, Z.M. Liu, Micropor. Mesopor. Mater. 60 (2003) 197–206.
[16] C.L. Sun, M.J. Peltre, M. Briend, J. Blanchard, K. Fajerwerg, J.M. Krafft, M. Breysse, M. Cattenot, M. Lacroix, Appl. Catal. A: Gen. 245 (2003) 245–255.
[17] G. Bergeret, P. Gallezot, in: G. Ertl, H. Knözinger, J. Weitkamp (Eds.), Handbook of Heterogeneous Catalysis, Wiley-VCH, p. 439.
[18] K.K. Bando, T. Saito, K. Sato, T. Tanaka, F. Dumeignil, M. Imamura, N. Matsubayashi, H. Shimada, J. Synchr. Radiat. 8 (2001) 581–583.
[19] B. Ravel, M. Newville, J. Synchr. Radiat. 12 (2005) 537–541.
[20] M. Newville, J. Synchr. Radiat. 8 (2001) 322–324.
[21] B. Ravel, J. Synchr. Radiat. 8 (2001) 314–316.
[22] J.J. Rehr, R.C. Albers, Rev. Mod. Phys. 72 (2000) 621–654.
[23] D. Bazin, I. Kovács, J. Lynch, L. Guczi, Appl. Catal. A: Gen. 242 (2003) 179–186.
[24] M. Vaarkamp, F.S. Modica, J.T. Miller, D.C. Koningsberger, J. Catal. 144 (1993) 611–626.
[25] D.C. Koningsberger, B.C. Gates, Catal. Lett. 14 (1992) 271–277.
[26] J. de Graaf, A.J. van Dillen, K.P. de Jong, D.C. Koningsberger, J. Catal. 203 (2001) 307–321.
[27] T. Matsui, M. Harada, K.K. Bando, M. Toba, Y. Yoshimura, Appl. Catal. A: Gen. 290 (2005) 73–80.
[28] T. Matsui, M. Harada, Y. Ichihashi, K.K. Bando, N. Matsubayashi, M. Toba, Y. Yoshimura, Appl. Catal. A: Gen. 286 (2005) 249–257.